

## Expansion Dynamics of a Shell-Shaped Bose-Einstein Condensate

Fan Jia<sup>1</sup>, Zerong Huang<sup>1</sup>, Liyuan Qiu<sup>1</sup>, Rongzi Zhou<sup>1</sup>, Yangqian Yan<sup>1,2</sup> and Dajun Wang<sup>1,2,\*</sup>

<sup>1</sup>Department of Physics, The Chinese University of Hong Kong, Hong Kong SAR, China

<sup>2</sup>The Chinese University of Hong Kong Shenzhen Research Institute, 518057 Shenzhen, China



(Received 3 August 2022; accepted 18 November 2022; published 9 December 2022)

We report the creation of a shell BEC in the presence of Earth's gravity with immiscible dual-species BECs of sodium and rubidium atoms. After minimizing the displacement between the centers of mass of the two BECs with a magic-wavelength optical dipole trap, the interspecies repulsive interaction ensures the formation of a closed shell of sodium atoms with its center filled by rubidium atoms. Releasing the double BEC together from the trap, we observe explosion of the filled shell accompanied by energy transfer from the inner BEC to the shell BEC. With the inner BEC removed, we obtain a hollow shell BEC that shows self-interference as a manifestation of implosion. Our results pave an alternative way for investigating many of the intriguing physics offered by shell BECs.

DOI: 10.1103/PhysRevLett.129.243402

**Introduction.**—Engineering the external trapping potential to emulate Hamiltonians governing vastly different physical systems is one of the main applications of Bose-Einstein condensates (BEC) of ultracold dilute atomic gases [1]. In the past two decades, BECs in optical lattices [2–4], in lower dimension 2D [5] and 1D traps [6], and in box potentials [7] have all been routinely created for investigating a broad range of physics. Another interesting path is creating BEC samples with nontrivial real-space topologies. For example, the persistent flow of toroidal BECs is linked to physics in the SQUID system [8,9], while its supersonic expansion is analogous to the cosmological expansion of the Universe [10]. BEC trapped on the surface of a sphere, dubbed the shell or bubble BEC, which was first proposed in 2001 [11], is another important case of BEC with nontrivial real-space topology. In recent years, many unique properties of the condensate caused by the topology of the shell structure have been predicted, including distinctive collective modes [12–14], interesting thermodynamic behaviors such as expansion induced cooling and depletion of the condensate [15–17], and the appearance of self-interference patterns due to implosion during free expansion [12,16]. For rotational velocity above a critical value, the closed shell leads to the formation of stable vortex-antivortex pairs [18]. In the thin-shell limit, the shell BEC can also undergo the Berezinskii-Kosterlitz-Thouless transition for revealing the connection between BEC and superfluid on curved spaces [15].

Despite these long-standing interests, experimental investigations on shell BECs are still an effort underway, mainly because of the challenge in their creation. The original proposal for generating the shell-shaped potential relies on the radio-frequency dressed magnetic trap [11,19]. Unfortunately, this potential is prone to gravity induced distortion that depletes the density at the top to zero [20].

Because of this, a microgravity environment, such as that found in the NASA Cold Atom Laboratory on board the International Space Station, has been assumed as a prerequisite for realizing the shell BEC [21]. Indeed, very recently, the first shell BEC was successfully created by the Cold Atom Laboratory project [22].

We present here the creation and investigation of the shell BEC using a very different method that relies on optically trapped double species BECs of <sup>23</sup>Na and <sup>87</sup>Rb atoms in the immiscible phase [23–26]. We found that <sup>23</sup>Na BECs in a fully closed shell can be formed robustly in the presence of Earth's gravity. This has allowed us to study the expansion dynamics of the shell BEC together with the center BEC or by itself. In the latter case, the implosion of the shell, which manifests as highly repeatable self-interference patterns, is observed [12,16].

In the 1990s, Ho *et al.* [23] and Pu *et al.* [24] had already pointed out that in the immiscible phase of the double BEC of <sup>23</sup>Na and <sup>87</sup>Rb atoms, the <sup>23</sup>Na BEC could form a shell surrounding the <sup>87</sup>Rb BEC. Recently, Wolf *et al.* revisited this idea [27]. In 2013, we produced the first double BEC of <sup>23</sup>Na and <sup>87</sup>Rb and confirmed that they are indeed immiscible near zero magnetic field [28,29]. Originally, the two condensates were cotrapped in an optical dipole trap (ODT) formed by crossing two 1070 nm laser beams. In the harmonic trap approximation, at this wavelength, the trap oscillation frequencies  $\omega$  are not the same. In the vertical (*y*) direction, this leads to a displacement between the centers of mass of the two BECs due to their different gravitational sags  $-g/\omega^2$ , where  $g$  is the gravitational acceleration. As a result, the <sup>23</sup>Na BEC has a crescent shape with a bottom notch repelled by the <sup>87</sup>Rb atoms [29]. Here, we solve this problem by changing the crossed ODT to the “magic” wavelength of 946 nm where the two

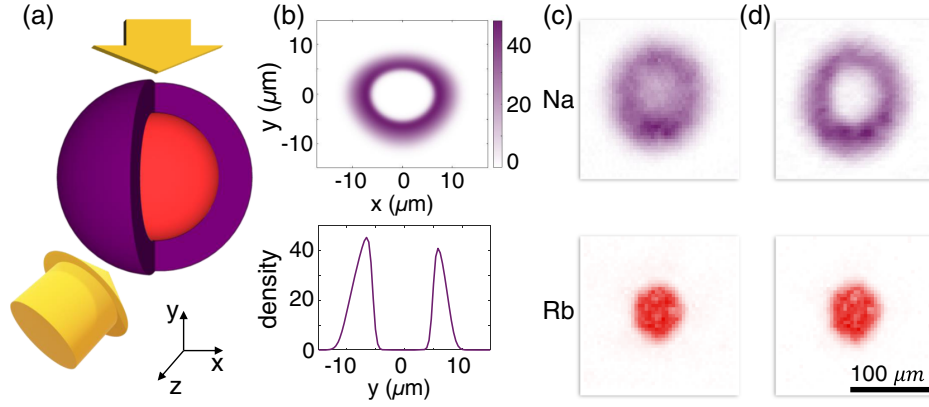


FIG. 1. Creating a shell-shaped BEC with the immiscible double BEC. (a) Schematic 3D distribution of the  $^{23}\text{Na}$  (purple) and  $^{87}\text{Rb}$  (red) atoms in the magic-wavelength crossed ODT. The probe beams (left-bottom arrow) for absorption imaging propagate along the  $z$  axis. The light sheet optical pumping beam for the shell (top arrow) is introduced from the vertical  $y$  direction. (b) The 2D contour plot of the  $^{23}\text{Na}$  shell in the  $x$ - $y$  plane (upper) and its 1D profile along the  $y$  axis (lower) from numerical simulation. In the presence of the  $y$ -axis asymmetry due to the gravity induced trapping potential distortion, a closed  $^{23}\text{Na}$  shell can still form. The upper images in (c) and (d) are OD images of the shell obtained with round and light sheet  $^{23}\text{Na}$  optical pumping beams, respectively. The shell structure is more clearly revealed in the latter configuration. All four images are obtained after coexpansion time  $t_{\text{co}} = 12$  ms. The same color code will be used throughout this Letter.

species have the same  $\omega$  [30]. They thus have the same amount of gravitational sags and nearly overlapping centers of mass.

In this magic-wavelength trap, the number density ratio  $n_2/n_1$  for two independent condensates is proportional to  $(U_{11}m_2/U_{22}m_1)^{3/5}$ , where  $U_{ij} = 2\pi\hbar^2 a_{ij}/\mu_{ij}$  are the interaction constants,  $m_i$  the atomic masses, and  $\mu_{ij} = m_i m_j / (m_i + m_j)$  the reduced masses (with  $i = 1$  and  $2$  for  $^{23}\text{Na}$  and  $^{87}\text{Rb}$ , respectively). We prepare  $^{23}\text{Na}$  ( $^{87}\text{Rb}$ ) in the  $|F = 1, m_F = -1\rangle$  hyperfine Zeeman state of which the  $s$ -wave scattering length is  $a_{11} = 54.6a_0$  [31] ( $a_{22} = 100.1a_0$  [32]). With  $a_{12} = 76.3a_0$  in low magnetic field [33], the  $^{23}\text{Na}$ - $^{87}\text{Rb}$  double BEC is in the immiscible phase with  $U_{12} > \sqrt{U_{11}U_{22}}$ . Since  $n_2/n_1 = 3.4$  for equal number of atoms, the lower density  $^{23}\text{Na}$  BEC will be pushed outward to further lower its density and reduce its overlap with  $^{87}\text{Rb}$  atoms to minimize the total interaction energy. The result of this buoyancy effect is a shell of  $^{23}\text{Na}$  BEC filled with  $^{87}\text{Rb}$  atoms, as illustrated schematically in Fig. 1(a).

The more detailed density distribution of the double BEC can be obtained by numerical simulation [34] of the coupled Gross-Pitaevskii equations [35]:

$$i\hbar \frac{\partial \psi_i}{\partial t} = \left[ -\frac{\hbar^2 \nabla^2}{2m_i} + V_i + U_{ii}n_i + U_{ij}n_j \right] \psi_i, \quad (1)$$

where  $V_i$  are the external trap potentials including contributions from both the ODT and gravity. After the evaporative cooling for creating the double BEC, although the centers of mass are nearly together,  $V_i$  are still severely distorted by gravity. The result of this complication is

reflected in the 2D contour plot of the calculated in-trap density of the  $^{23}\text{Na}$  BEC in the  $x$ - $y$  plane as presented in the upper panel of Fig. 1(b), which indicates that a closed, but not perfectly symmetrical shell is indeed formed. It becomes even more obvious in the 1D density distribution sliced along the vertical direction. For example, the lower panel of Fig. 1(b) shows that more atoms are located at the bottom than at the top part of the shell. Nevertheless, our simulation shows that, for a large range of atom number ratios, fully closed  $^{23}\text{Na}$  BEC shells can still be formed readily.

*Detection of the shell structure.*—Our experiment starts from double BECs prepared in the crossed-beam magic-wavelength ODT with typically  $1.3 \times 10^5$   $^{23}\text{Na}$  atoms and  $1.2 \times 10^5$   $^{87}\text{Rb}$  atoms. At the final stage of the evaporative cooling, the measured trap oscillation frequency is  $2\pi \times 108 \text{ s}^{-1}$  ( $2\pi \times 85 \text{ s}^{-1}$ ) in the vertical (radial) direction. To detect the atoms, first, we abruptly switch off the trapping laser beams followed by time-of-flight (TOF) expansion. Second, atoms are transferred from the  $F = 1$  hyperfine states to the  $F = 2$  states by an optical pumping beam. For  $^{87}\text{Rb}$ , the state transfer is done with either an optical pumping beam or a 6.8 GHz microwave. Finally, we detect the atoms by absorption imaging using probe beams on the  $F = 2 \rightarrow F' = 3$  cycling transitions. Thanks to the drastically different transition wavelengths, we not only achieve species-selective detection in nearly the same instant but also can study the expansion dynamics of one of the species by removing the other one. Hereafter, we will use  $t_{\text{co}}$  to denote the expansion time of the filled shell (or in other words, coexpansion time of the double BEC), and  $t_s^{\text{Na}}$  ( $t_s^{\text{Rb}}$ ) to represent the additional expansion time of the  $^{23}\text{Na}$

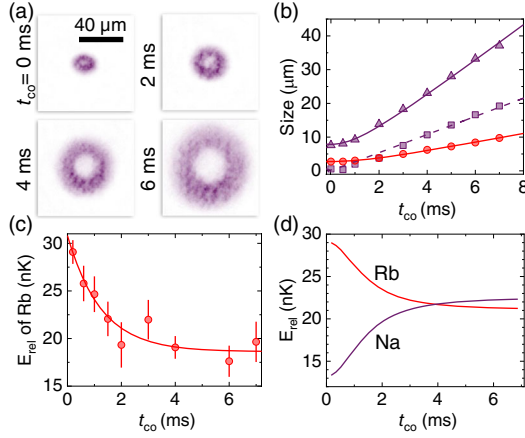


FIG. 2. Expansion dynamics of the  $^{23}\text{Na}$  shell filled with the  $^{87}\text{Rb}$  BEC. (a),(b) OD images and the extracted inner (squares) and outer (triangles) sizes of the  $^{23}\text{Na}$  shell versus coexpansion time  $t_{\text{co}}$ . For the first 2 ms, the size of the  $^{87}\text{Rb}$  BEC (filled circles) is nearly the same as the inner size of the shell. (c)  $E_{\text{rel}}$  of the  $^{87}\text{Rb}$  BEC after coexpansion with the shell. The solid curve is fit to the shifted exponential decay with a time constant of 1.3(4) ms. (d) The numerical simulation confirms the energy transfer from the inner  $^{87}\text{Rb}$  BEC to the  $^{23}\text{Na}$  shell.

( $^{87}\text{Rb}$ ) BEC after the  $^{87}\text{Rb}$  ( $^{23}\text{Na}$ ) BEC is removed. The total TOF after shutting off the ODT is thus  $t_{\text{tof}} = t_{\text{co}} + t_{\text{s}}^{\text{Na/Rb}}$ .

Figure 1(c) shows the absorption images of the  $^{23}\text{Na}$  and  $^{87}\text{Rb}$  BECs after  $t_{\text{co}}$  of 12 ms. Because of the integration along the probing direction, the shell structure of the  $^{23}\text{Na}$  BEC manifests only as a lower optical density (OD) in the center. To obtain more detailed information of the shell, we change the  $^{23}\text{Na}$  optical pumping beam to a light sheet [34,36] of 15  $\mu\text{m}$  thick and 800  $\mu\text{m}$  wide. In this configuration, only a thin slice of the  $^{23}\text{Na}$  atoms in the center part of the shell can be detected by the probe beam. The  $^{23}\text{Na}$  shell thus shows up as a ring in the image as can be seen in Fig. 1(d). However, as shown in Fig. 2(a), since the thickness of the light sheet is limited, to resolve the hollow  $^{23}\text{Na}$  shell,  $t_{\text{tof}}$  needs to be longer than 2 ms, when the inner radius of the shell becomes larger following the expansion. For the best performance, the focus of light sheet is adjusted to follow the shell at different  $t_{\text{tof}}$ .

*Expansion dynamics of the filled shell.*—Because of the repulsive interspecies interaction, the filled  $^{23}\text{Na}$  shell expands outward and its outer and inner sizes increase with  $t_{\text{co}}$ , as shown in Figs. 2(a) and 2(b). Correspondingly, the outward expansion of the  $^{87}\text{Rb}$  BEC is also affected by the  $^{23}\text{Na}$  shell, which, not surprisingly, is different from the typical BEC expansion in free space. To reveal this point, we measure the release energy  $E_{\text{rel}}$  [34,37–39] of the  $^{87}\text{Rb}$  BEC after different  $t_{\text{co}}$ . We first let the  $^{87}\text{Rb}$  BEC coexpand with the  $^{23}\text{Na}$  shell and then remove the  $^{23}\text{Na}$  shell in less than 100  $\mu\text{s}$ . Afterward, the  $^{87}\text{Rb}$  BEC starts to expand in free space and its  $E_{\text{rel}}$  is extracted from the expansion

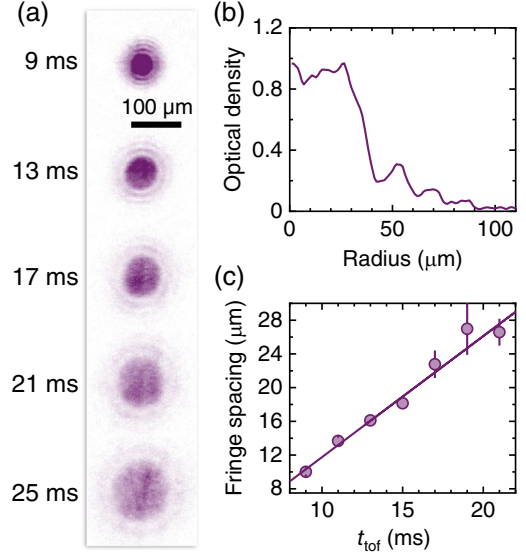


FIG. 3. Self-interference of the hollow shell BEC. (a) OD images at different  $t_{\text{tof}}$  for the  $^{23}\text{Na}$  shell created after coexpansion time  $t_{\text{co}} = 0.3$  ms. The implosion of the shell leads to self-interference. The contrast of the images is adjusted to enhance the visibility of the fringes. (b) Azimuthally averaged profile of the  $^{23}\text{Na}$  shell at  $t_{\text{tof}} = 15$  ms. The center peak is flattop and the contrast of the first fringe located near 50  $\mu\text{m}$  is about 30%. (c) The measured fringe spacing versus  $t_{\text{tof}}$ . The solid line is a linear fit to the data.

velocity after further TOF  $t_{\text{s}}^{\text{Rb}}$ . As shown in Fig. 2(c), initially  $E_{\text{rel}}$  decreases rapidly with  $t_{\text{co}}$ , i.e., the  $^{87}\text{Rb}$  BEC is losing energy during the coexpansion. At longer  $t_{\text{co}}$ ,  $E_{\text{rel}}$  finally levels off. During this whole process, about 40% of the initial  $E_{\text{rel}}$  are lost. Empirically, we find that the data are fitted very well to a shifted exponential decay with a time constant  $\tau = 1.3(4)$  ms.

Since the total energy of the double BEC is conserved, the lost energy of the  $^{87}\text{Rb}$  BEC can only be absorbed by the  $^{23}\text{Na}$  shell, i.e., the expansion of the filled shell is accompanied by energy transfer between the two species. This is analogous to the energy transfer between coupled oscillators, only here it is irreversible due to the free expansion of the shell. The energy transfer rate, which is reflected in the loss rate of  $E_{\text{rel}}$ , is proportional to the interspecies interaction energy. It is thus fastest at shorter  $t_{\text{co}}$  and slows down when the interaction energy is weakened following the expansion. This picture agrees with the observation in Fig. 2(c), which is confirmed by numerical simulations of the coupled Gross-Pitaevskii equations plotted in Fig. 2(d). The simulation also confirms that indeed the energy of the  $^{23}\text{Na}$  shell increases during the filled expansion.

*Self-interference of the hollow shell.*—Next, we study the very different expansion dynamics of the hollow  $^{23}\text{Na}$  shell. To this end, after some initial filled expansion time  $t_{\text{co}}$ , we remove the  $^{87}\text{Rb}$  atoms in 100  $\mu\text{s}$  by pulses of the optical

pumping beam and the probing beam. During and after this removal process, we observe no indications that the  $^{23}\text{Na}$  shell is affected. Figure 3(a) demonstrates the absorption images at several  $t_{\text{tof}}$  for the shell created after 0.3 ms of  $t_{\text{co}}$ . Different from the filled expansion, here the  $^{23}\text{Na}$  shell expands both outward and inward. When  $^{23}\text{Na}$  atoms reach the center following the inward implosion, the signature self-interference of the shell BEC [12,16] is observed. Figure 3(b) shows the partially azimuthally averaged OD [34] versus distance from the shell center for  $t_{\text{tof}} = 15$  ms. Two important features can be clearly identified. First, the majority of the  $^{23}\text{Na}$  atoms accumulate at the center and form a broad peak with a nearly flattop high density distribution. Second, concentric interference fringes with much lower densities appear. Both features are in full agreement with theoretical predictions [12,16,27]. Typically, the first fringe shows up as a nearly fully closed ring while fragments of the third fringe are still visible. The measured contrasts of the fringes are up to 30%. Considering the light sheet optical pumping beam and the symmetry of the shell, it is conceivable that the first fringe forms a nearly spherical and probably closed shell. For the higher order fringes, only broken shells are formed, most probably due to the imperfect spherical symmetry of the shell.

From shot to shot, the main features of the self-interference patterns are highly repeatable because of the fixed relative phase in the initial wave function. This is in stark contrast to the interference between two completely independent BECs in which the fringes vary from shot to shot due to the separated phase evolution of the two BECs [36,40]. However, in both cases, the fringe spacing  $\delta$  increases linearly for long TOF. For the shell BEC, we have [12,41]

$$\delta = \frac{h t_s^{\text{Na}}}{2r_0 m_{\text{Na}}}, \quad (2)$$

with  $2r_0$  an initial diameter of the shell, and  $h$  the Planck constant. This equation is derived for noninteracting systems [40], which is applicable here since the densities in the fringes are low. Figure 3(c) shows  $\delta$  extracted from the images in Fig. 3(a). From a linear fit to Eq. (2) with an offset, the fringe spacing increases with a rate of 1.31(4)  $\mu\text{m}/\text{ms}$ , which is consistent with the simulated value of 1.13  $\mu\text{m}/\text{ms}$ .

The self-interference can be tuned by changing the initial  $t_{\text{co}}$ . Shown in Fig. 4 are images of the  $^{23}\text{Na}$  shell with fixed  $t_{\text{tof}}$  of 20 ms for initially hollow shells created at  $t_{\text{co}}$  from 0.1 to 5 ms. With increasing  $t_{\text{co}}$ , the number of atoms accumulated at the center reduces continuously and vanishes completely at 2.5 ms. For even longer  $t_{\text{co}}$ , an obvious implosion can no longer be observed. The visibility of the self-interference fringes also decreases with increasing  $t_{\text{co}}$  and disappears at around 1 ms.

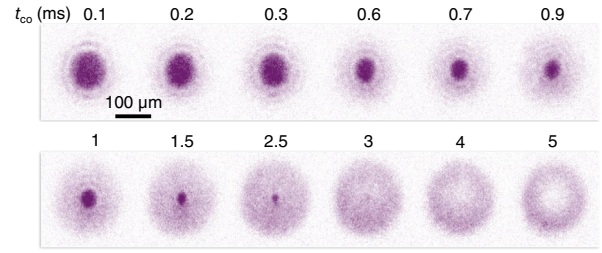


FIG. 4. Controlling the expansion dynamics of the hollow shell. The self-interference patterns for shells formed after different coexpansion time  $t_{\text{co}}$  are shown. The total TOF  $t_{\text{tof}}$  is fixed to 20 ms. The contrast of the images is adjusted to enhance the visibility.

These behaviors can be interpreted by the aforementioned energy transfer during the filled expansion. For the first 2 ms, the  $^{23}\text{Na}$  shell gains more and more energy, so both its inner and outer surfaces will expand outward with faster and faster velocities. After the  $^{87}\text{Rb}$  BEC is removed, the motion of the inner surface of the  $^{23}\text{Na}$  shell has to be reversed for implosion to happen. Thus, at the moment when implosion starts,  $r_0$  will be larger for longer  $t_{\text{co}}$ . This will result in less accumulation of atoms at the center and, following Eq. (2), a smaller  $\delta$  makes the fringes harder to be resolved due to the limited imaging resolution, even if they are still there. Presumably, these fringes should become observable after longer TOF and with the help of the matter-wave lensing method [42]. Eventually, for even longer  $t_{\text{co}}$ , when most of the internal energy of the  $^{23}\text{Na}$  BEC has been converted into kinetic energy of the outward motion, there is simply not enough energy left to reverse the motion for implosion to happen.

*Summary and outlook.*—In the current system, the shell BEC is still not in the thin-shell limit that is the focus of most theoretical works [12–17]. However, many features of the shell BEC, including the distinctive collective excitation modes [12,24,27] and the vortex dynamics [18], can still be explored. The double BEC system also provides many additional flexibilities. For instance, the in-trap shell thickness can be reduced by increasing the number ratio between the inner BEC and the shell BEC [24]. For the current  $^{23}\text{Na}$ - $^{87}\text{Rb}$  system, the previously observed Feshbach resonances [28,33] can be exploited to tune the interspecies interaction. This can be used to change the sign of the interspecies interaction for studying the shell implosion in different regimes or even the shell to quantum droplet [39] transition.

During the review process, we learned that a full shell was created using the rf dressed potential by compensating the gravity with the inhomogeneity of the rf coupling [43].

We thank Zhichao Guo for the valuable discussions. This work was supported by the Hong Kong RGC General Research Fund (Grants 14301620 and 14301818), the Collaborative Research Fund (Grants C6005-17G and C6009-20GF) and CUHK Direct Grant No. 4053535.

\*Corresponding author.

djiang@cuhk.edu.hk

- [1] I. Bloch, J. Dalibard, and W. Zwerger, Many-body physics with ultracold gases, *Rev. Mod. Phys.* **80**, 885 (2008).
- [2] M. Greiner, O. Mandel, T. Esslinger, T. W. Hänsch, and I. Bloch, Quantum phase transition from a superfluid to a mott insulator in a gas of ultracold atoms, *Nature (London)* **415**, 39 (2002).
- [3] I. Bloch, J. Dalibard, and S. Nascimbene, Quantum simulations with ultracold quantum gases, *Nat. Phys.* **8**, 267 (2012).
- [4] C. Gross and I. Bloch, Quantum simulations with ultracold atoms in optical lattices, *Science* **357**, 995 (2017).
- [5] Z. Hadzibabic and J. Dalibard, Two-dimensional Bose fluids: An atomic physics perspective, *Riv. Nuovo Cimento* **34**, 389 (2011).
- [6] M. A. Cazalilla, R. Citro, T. Giamarchi, E. Orignac, and M. Rigol, One dimensional bosons: From condensed matter systems to ultracold gases, *Rev. Mod. Phys.* **83**, 1405 (2011).
- [7] N. Navon, R. P. Smith, and Z. Hadzibabic, Quantum gases in optical boxes, *Nat. Phys.* **17**, 1334 (2021).
- [8] A. Ramanathan, K. C. Wright, S. R. Muniz, M. Zelan, W. T. Hill, C. J. Lobb, K. Helmerson, W. D. Phillips, and G. K. Campbell, Superflow in a Toroidal Bose-Einstein Condensate: An Atom Circuit with a Tunable Weak Link, *Phys. Rev. Lett.* **106**, 130401 (2011).
- [9] K. C. Wright, R. B. Blakestad, C. J. Lobb, W. D. Phillips, and G. K. Campbell, Driving Phase Slips in a Superfluid Atom Circuit with a Rotating Weak Link, *Phys. Rev. Lett.* **110**, 025302 (2013).
- [10] S. Eckel, A. Kumar, T. Jacobson, I. B. Spielman, and G. K. Campbell, A Rapidly Expanding Bose-Einstein Condensate: An Expanding Universe in the Lab, *Phys. Rev. X* **8**, 021021 (2018).
- [11] O. Zobay and B. M. Garraway, Two-Dimensional Atom Trapping in Field-Induced Adiabatic Potentials, *Phys. Rev. Lett.* **86**, 1195 (2001).
- [12] C. Lannert, T. C. Wei, and S. Vishveshwara, Dynamics of condensate shells: Collective modes and expansion, *Phys. Rev. A* **75**, 013611 (2007).
- [13] K. Padavić, K. Sun, C. Lannert, and S. Vishveshwara, Physics of hollow Bose-Einstein condensates, *Europhys. Lett.* **120**, 20004 (2017).
- [14] K. Sun, K. Padavić, F. Yang, S. Vishveshwara, and C. Lannert, Static and dynamic properties of shell-shaped condensates, *Phys. Rev. A* **98**, 013609 (2018).
- [15] A. Tononi and L. Salasnich, Bose-Einstein Condensation on the Surface of a Sphere, *Phys. Rev. Lett.* **123**, 160403 (2019).
- [16] A. Tononi, F. Cinti, and L. Salasnich, Quantum Bubbles in Microgravity, *Phys. Rev. Lett.* **125**, 010402 (2020).
- [17] B. Rhyno, N. Lundblad, D. C. Aveline, C. Lannert, and S. Vishveshwara, Thermodynamics in expanding shell-shaped Bose-Einstein condensates, *Phys. Rev. A* **104**, 063310 (2021).
- [18] K. Padavić, K. Sun, C. Lannert, and S. Vishveshwara, Vortex-antivortex physics in shell-shaped Bose-Einstein condensates, *Phys. Rev. A* **102**, 043305 (2020).
- [19] O. Zobay and B. M. Garraway, Atom trapping and two-dimensional Bose-Einstein condensates in field-induced adiabatic potentials, *Phys. Rev. A* **69**, 15 (2004).
- [20] Y. Guo, R. Dubessy, M. d. G. de Herve, A. Kumar, T. Badr, A. Perrin, L. Longchambon, and H. Perrin, Supersonic Rotation of a Superfluid: A Long-Lived Dynamical Ring, *Phys. Rev. Lett.* **124**, 025301 (2020).
- [21] N. Lundblad, R. A. Carollo, C. Lannert, M. J. Gold, X. Jiang, D. Paseltiner, N. Sergay, and D. C. Aveline, Shell potentials for microgravity Bose-Einstein condensates, *npj Microgravity* **5**, 1 (2019).
- [22] R. A. Carollo, D. C. Aveline, B. Rhyno, S. Vishveshwara, C. Lannert, J. D. Murphree, E. R. Elliott, J. R. Williams, R. J. Thompson, and N. Lundblad, Observation of ultracold atomic bubbles in orbital microgravity, *Nature (London)* **606**, 281 (2022).
- [23] T.-L. Ho and V. B. Shenoy, Binary Mixtures of Bose Condensates of Alkali Atoms, *Phys. Rev. Lett.* **77**, 3276 (1996).
- [24] H. Pu and N. P. Bigelow, Properties of Two-Species Bose Condensates, *Phys. Rev. Lett.* **80**, 1130 (1998).
- [25] M. Trippenbach, K. Góral, K. Rzazewski, B. Malomed, and Y. B. Band, Structure of binary Bose-Einstein condensates, *J. Phys. B* **33**, 4017 (2000).
- [26] K. L. Lee, N. B. Jørgensen, I. K. Liu, L. Wacker, J. J. Arlt, and N. P. Proukakis, Phase separation and dynamics of two-component Bose-Einstein condensates, *Phys. Rev. A* **94**, 1 (2016).
- [27] A. Wolf, P. Boegel, M. Meister, A. Balaž, N. Gaaloul, and M. A. Efremov, Shell-shaped Bose-Einstein condensates based on dual-species mixtures, *Phys. Rev. A* **106**, 013309 (2022).
- [28] F. Wang, D. Xiong, X. Li, D. Wang, and E. Tiemann, Observation of Feshbach resonances between ultracold Na and Rb atoms, *Phys. Rev. A* **87**, 1 (2013).
- [29] F. Wang, X. Li, D. Xiong, and D. Wang, A double species  $^{23}\text{Na}$  and  $^{87}\text{Rb}$  Bose-Einstein condensate with tunable miscibility via an interspecies Feshbach resonance, *J. Phys. B* **49**, 015302 (2016).
- [30] M. S. Safronova, B. Arora, and C. W. Clark, Frequency-dependent polarizabilities of alkali-metal atoms from ultraviolet through infrared spectral regions, *Phys. Rev. A* **73**, 022505 (2006).
- [31] S. Knoop, T. Schuster, R. Scelle, A. Trautmann, J. Appmeier, M. K. Oberthaler, E. Tiesinga, and E. Tiemann, Feshbach spectroscopy and analysis of the interaction potentials of ultracold sodium, *Phys. Rev. A* **83**, 042704 (2011).
- [32] E. G. M. van Kempen, S. J. J. M. F. Kokkelmans, D. J. Heinzen, and B. J. Verhaar, Interisotope Determination of Ultracold Rubidium Interactions from Three High-Precision Experiments, *Phys. Rev. Lett.* **88**, 093201 (2002).
- [33] Z. Guo, F. Jia, B. Zhu, L. Li, J. M. Hutson, and D. Wang, Improved characterization of Feshbach resonances and interaction potentials between  $^{23}\text{Na}$  and  $^{87}\text{Rb}$  atoms, *Phys. Rev. A* **105**, 023313 (2022).
- [34] See Supplemental Material at <http://link.aps.org/supplemental/10.1103/PhysRevLett.129.243402> for more details on the trapping potential, the detection method, and the data processing.

- [35] X. Antoine and R. Duboscq, GPELab, a Matlab toolbox to solve Gross-Pitaevskii equations I: Computation of stationary solutions, *Comput. Phys. Commun.* **185**, 2969 (2014).
- [36] M.R. Andrews, C.G. Townsend, H.-J. Miesner, D.S. Durfee, D.M. Kurn, and W. Ketterle, Observation of interference between two Bose condensates, *Science* **275**, 637 (1997).
- [37] M.-O. Mewes, M.R. Andrews, N.J. van Druten, D.M. Kurn, D.S. Durfee, and W. Ketterle, Bose-Einstein Condensation in a Tightly Confining dc Magnetic Trap, *Phys. Rev. Lett.* **77**, 416 (1996).
- [38] M.J. Holland, D.S. Jin, M.L. Chiofalo, and J. Cooper, Emergence of Interaction Effects in Bose-Einstein Condensation, *Phys. Rev. Lett.* **78**, 3801 (1997).
- [39] Z. Guo, F. Jia, L. Li, Y. Ma, J.M. Hutson, X. Cui, and D. Wang, Lee-Huang-Yang effects in the ultracold mixture of  $^{23}\text{Na}$  and  $^{87}\text{Rb}$  with attractive interspecies interactions, *Phys. Rev. Res.* **3**, 1 (2021).
- [40] A. Röhrl, M. Naraschewski, A. Schenzle, and H. Wallis, Transition from Phase Locking to the Interference of Independent Bose Condensates: Theory versus Experiment, *Phys. Rev. Lett.* **78**, 4143 (1997).
- [41] F. Dalfovo, S. Giorgini, L.P. Pitaevskii, and S. Stringari, Theory of Bose-Einstein condensation in trapped gases, *Rev. Mod. Phys.* **71**, 463 (1999).
- [42] P. Boegel, A. Wolf, M. Meister, and M. A. Efremov, Matter-wave lensing of shell-shaped Bose-Einstein condensates, [arXiv:2209.04672](https://arxiv.org/abs/2209.04672).
- [43] Y. Guo, E.M. Gutierrez, D. Rey, T. Badr, A. Perrin, L. Longchambon, V.S. Bagnato, H. Perrin, and R. Dubessy, Expansion of a quantum gas in a shell trap, *New J. Phys.* **24**, 093040 (2022).